Structure−Activity Relationship in HC-SCR of NO_x by TEM, O_2-Chemisorption, and EDXS Study of Ag/Al_2O_3

K. Arve,[†] K. Svennerberg,[‡] F. Klingstedt,[†] K. Eränen,[†] L. R. Wallenberg,[‡] J.-O. Bovin,[‡] L. Čapek,[§] and D. Yu. Murzin*[,†]

Laboratory of Industrial Chemistry, Process Chemistry Centre, Åbo Akademi University, Åbo, Finland, Department of Materials Chemistry, Kemicentrum, Lund Institute of Technology, Lund University, Lund, Sweden, and J. Heyrovsky Institute of Physical Chemistry, Prague, Czech Republik

Received: September 12, 2005; In Final Form: November 4, 2005

Ag/alumina catalysts with different silver loading (1.28−6 wt %) for lean NO reduction activity were prepared by impregnation and the incipient wetness method. Complementary HRTEM, HAADF, O_2-chemisorption, and EDXS studies were applied to investigate the dependence between silver particle size and catalytic activities of the prepared materials. The catalyst with the lowest silver loading (1.28 wt %) was found to be the most active catalyst in terms of reacted NO molecules per mole of silver. On the basis of the HRTEM, HAADF, and O_2-chemisorption studies it could be concluded that the mean particle size or particle size distribution of the samples alone could not explain the big difference in the activities. EDXS analyses showed on the other hand that all of the samples were very heterogeneous in terms of particle size distribution, e.g., including both small and very big particles. Furthermore, both metallic silver and mainly hexagonal silver oxide (Ag_2O) were found to be present in the samples. Despite the valuable information provided by ex situ characterization of the prepared samples, it needs to be emphasized that establishing a structure−reactivity relationship for this type of catalyst requires in situ characterization.

1. Introduction

Selective catalytic reduction of NO_x by hydrocarbons under an excess of oxygen has been widely studied for its potential to clean up exhausts from lean burn and diesel engines. Since the early work of Iwamoto et al.[1] and Held et al.[2] with Cu-ZSM-5, silver supported on alumina has been reported to be an active and stable catalyst for selective catalytic reduction of nitrogen oxides with various hydrocarbons (HC-SCR).[3−19] Discussions have occurred about the optimal silver loading on the alumina support. It has been shown that the best catalytic performance is obtained at low and intermediate silver loadings (1.2−3 wt %), while higher amounts of silver lead to undesired total combustion of hydrocarbons.[7−12,18] Such dependence on silver content indicates that the particle size and dispersion of silver play an important role in the active catalysts. Hoost et al.[8] found an optimal silver loading of about 2 wt % on γ-alumina (Degussa C γ-alumina). However, Iglesias-Juez et al.[12] have shown that 4.5 wt % silver on alumina (Condea, B.E.T. 200 m^2/g for calcined sample), prepared by the pH controlled incipient wetness method, is an active catalyst in C_3H_6-NO_x. Moreover, Luo et al.[14] have prepared an active Ag/alumina catalyst containing 5 wt % silver by a sol−gel method (B.E.T. 172 m^2/g for calcined sample). Thus it can be concluded that besides the amount of silver on the alumina support per se, there are other contributing factors for achieving a high NO_x reduction rate over Ag/alumina catalysts.

The relationship between the state of silver and the high NO_x to N_2 reduction activity over Ag/alumina catalysts has also been widely discussed in the literature.[7,9−12] Shimizu et al.[10] have reported UV−vis diffuse reflectance spectra for impregnated Ag/alumina catalysts having a varying silver loading (0.6, 2, 3, and 5 wt %). In their study[10] Ag^+ ions were found to be highly dispersed on the alumina support independent of the Ag loading. The main difference between the catalyst with the highest silver loading and the other prepared catalysts was the shoulder observed in the UV−vis spectrum around 280−350 nm for the 5 wt % catalyst. According to Shimizu et al.[10] this shoulder in the spectrum is attributed to Ag(0) clusters. Similar results have also been reported in ref 12. Bogdanchikova et al.[11] assigned in their study peaks at 290 and 350 nm to small Ag^+ clusters and the absorption at wavelengths higher than 390 nm to metallic silver Ag(0) particles. Thus, UV−vis studies should be compared very carefully with each other taking into account the metal loadings in the catalysts and the atmosphere in which the spectrum is scanned as it can affect the results.

XRD power spectra have also been used for characterizing Ag/alumina catalysts,[9,11−12] concluding formation of silver aluminate. However, it should be kept in mind that XRD is a technique applied primarily on large particles. Iglesias-Juez et al.[12] have shown by Fourier Transform of EXAFS that only a minor part of the silver atoms undergoes sintering during calcination and reaction, and that three different Ag-O contributions, referring to Ag^+, exist, where the active phase is connected to small silver aluminate particles possessing tetrahedral symmetry.

In supported metal catalysts the performance of a catalyst is related to the amount of active phase. Hence, it is also important to determine the sizes and size distributions of the metal nanoparticles. In this paper, the particle size (nm) and silver dispersion (%) have been evaluated globally (e.g., average values) and locally for four calcined Ag/alumina catalysts with

* Address correspondence to this author. E-mail: dmurzin@abo.fi.
[†] Åbo Akademi University.
[‡] Lund University.
[§] J. Heyrovsky Institute of Physical Chemistry.

10.1021/jp055147x CCC: $33.50
Published on Web 12/10/2005

TABLE 1: NO to N_2 conversions and NO rates Over the Prepared Catalysts at 350, 400, 450, and 500 °C

	350 °C		400 °C		450 °C		500 °C	
sample	conv (%)	rate[a]	conv (%)	rate[a]	conv (%)	rate[a]	conv (%)	rate[a]
1. Ag/Al_2O_3-1.28	33.5	2.6×10^{-5}	85.3	7.1×10^{-5}	94.8	8.4×10^{-5}	97.3	9.3×10^{-5}
2. Ag/Al_2O_3-1.91	36.4	1.9×10^{-5}	84.0	4.7×10^{-5}	97.9	5.8×10^{-5}	99.1	6.3×10^{-5}
3. Ag/Al_2O_3-2.88	28.0	9.5×10^{-6}	63.0	2.3×10^{-5}	80.5	3.2×10^{-5}	81.2	3.4×10^{-5}
4. Ag/Al_2O_3-6.00	0.6	9.8×10^{-8}	4.7	8.3×10^{-7}	7.2	1.4×10^{-6}	4.5	9.1×10^{-7}

[a] The rate is calculated as the amount of reacted moles of NO per gram of silver per second.

a varying (1.28−6.00 wt %) silver loading. The obtained results have been correlated to the NO_x to N_2 reduction activities over the examined catalysts. The mean particle size and particle size distribution of silver were studied by means of transmission electron microscopy (TEM) imaging, high angle annular dark field (HAADF) imaging, O_2-chemisorption, and X-ray energy dispersive spectroscopy (EDXS). The state of silver (silver oxide or metallic silver) cannot directly be determined from the TEM figures. However, a power spectrum (digital diffraction pattern) can be obtained from Fast Fourier Transformation (FFT) operations on a TEM image. In this work the distances in the diffraction patterns were measured and compared to distances reported in the literature[23−25] obtained from XRD measurements on silver and silver oxide (AgO, Ag_2O) to reveal information about the state of silver on the support. Application of high-resolution TEM for characterization of heterogeneous catalysts has been discussed in several papers,[26−28] but no comprehensive HR-TEM study devoted to silver supported on alumina for HC-SCR has been published in the open literature.

2. Experimental Section

2.1. Catalyst Preparation. Alumina supported silver catalysts with varying silver loading were prepared by impregnating a commercial (LaRoche) alumina support (<250 μm, B.E.T. 289 m^2/g), which is a mixture of χ, ρ, η, and pseudo-γ phases, with aqueous silver nitrate solution of high purity (J. T. Baker). Ag-nitrate concentrations of 0.011, 0.022, and 0.033 M were used and the time of impregnation was 24 h. In addition a high loaded Ag/alumina catalyst with 6.00 wt % Ag was prepared by the incipient wetness method. Thereafter the catalysts were dried for 3 h at 100 °C and calcination was carried out at 550 °C for 3 h in air. After the calcination the B.E.T for the samples were measured to be approximately 185 m^2/g. Catalysts are denoted according to their metal loading (wt %) as Ag/Al_2O_3-1.28, Ag/Al_2O_3-1.91, Ag/Al_2O_3-2.88, and Ag/Al_2O_3-6.00.

The overall uptake of silver by alumina was analyzed (XRF: X-MET 880, Outokumpu Electronics) by measuring the silver content in the precursor solution prior to and after impregnation.

2.2. Catalyst Activity Test. The Ag/alumina grains (0.4 g, diameter distribution 250−500 μm) were tested according to the same procedure as described in ref 18. GHSV = 60 000 h^{-1} (total flow of 550 mL/min) and a temperature range of 150−600 °C were used for the catalytic activity runs. The gas mixture used in the activity tests consisted of 500 ppm of NO, 375 ppm of *n*-octane, 6 vol % of O_2, 10 vol % of CO_2, 350 ppm of CO, 12 vol % of H_2O, and He as balance. NO_x to N_2 reduction activities (%) and turnover frequencies (s^{-1}) (moles of NO reacted per mole of silver per second) of the prepared catalysts were calculated at 400−500 °C and are given in Table 1.

2.3. Catalyst Characterization. *TEM.* Bright field transmission electron microscopy (TEM) images and high-angle annular dark field (HAADF, $\theta > 50$ mrad off axis) images of calcined non-reduced samples were used for determination of the mean particle size (MPS) and the particle size distribution for the Ag/alumina catalysts above. The particle size was calculated as the diameter of the particle in nanometers (nm) assuming spherical particle form. The equipment applied was a JEOL 3000F FEG-(S)TEM equipped with an X-ray energy dispersive spectroscopy (EDXS) system and a scanning transmission electron microscopy (STEM) unit. The electron source of a FEG-TEM is a field emission gun, which offers higher brightness, higher coherency, and a narrow energy spread in comparison to a thermionic gun. The accelerating voltage for the microscope is 300 kV and the point resolution is 1.65 Å. The point resolution for the HAADF unit is 1.4 Å. Ronchigrams were utilized for focus correction in HAADF imaging. Furthermore, TEM and HAADF images from each sample acquired from the same sample area were used to calibrate the magnification for the HAADF unit to attain correct values for the particle size determination. Crushed samples were placed on a copper grid covered with a thin lacy carbon film.

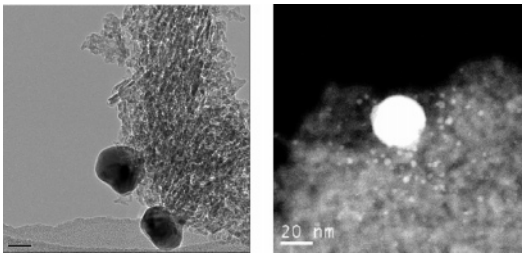

Figure 1. A bright field TEM image (left) vs a *Z* contrast image (right) illustrating the difference in contrast between silver particles (one marked with an arrow) and the alumina support.

TABLE 2: Results from Statistical Calculations Based on TEM Images

sample	silver content (wt %)	particle measured	MPS (nm)	standard deviation	confidence interval
1	1.28	115	5.36	10.02	5.36 ± 1.85
2	1.91	107	5.46	9.93	5.46 ± 1.90
3	2.88	112	8.54	11.01	8.54 ± 2.06
4	6.00	113	10.46	11.43	10.46 ± 2.13

With the HAADF (*Z* contrast images) imaging technique, it is possible to acquire images with suppressed diffraction contrast and enhanced mass-thickness contrast.[22] HAADF was utilized to capture images with a high contrast between silver and alumina. The reason for this was the unexpected low contrast between alumina and silver found in bright-field TEM images. In HAADF images, smaller silver particles were detectable than in corresponding TEM images (Figure 1). In HAADF images silver appears as brighter regions due to its higher *Z* value compared with alumina.

The mean particle size (MPS) for each sample was determined separately both from TEM and HAADF images (Tables 2 and 3). For each sample, a selection of around 100 particles was masked and the diameter (nm) of each particle was computed. The software used for the masking of the particles and the computations was Gatan Digital Micrograph 3.7.0. Bogdanchikova et al.[11] did not observe any reduction of silver cations, which would lead to increased particle size, in the course of

TABLE 3: Results from the Statistical Calculations Based on HAADF Images

sample	silver content (wt %)	particles measured	MPS (nm)	standard deviation	confidence interval
1	1.28	108	5.05	2.20	5.05 ± 0.42
2	1.91	101	5.08	9.11	5.08 ± 1.80
3	2.88	109	3.17	3.28	3.17 ± 0.62
4	6.00	107	4.25	5.66	4.25 ± 1.08

their characterization work with TEM. It is reasonable to make the same assumption for the experiments performed for this article.

O_2-Chemisorption. The global dispersion (%) of silver and mean particle size (nm) of the silver in the prepared catalysts were also determined by O_2-adsorption at 170 °C (Carlo Erba Instruments 1900) at a pressure range of 1 to 200 Torr of oxygen, according to ref 8. Before the chemisorption experiments the samples were reduced in a hydrogen stream (30 mL/min) by heating from room temperature to 250 °C with a heating rate of 5 °C/min, and then kept at this temperature for 2 h. The amount of the reversibly adsorbed oxygen on the catalysts was determined by the back-adsorption method. Metal dispersion and mean particle diameter (Table 4) were calculated by the Langmuir method according to the method adapted from the literature.[8] At the same time one should keep in mind that the degree of reduction is approximately 50% (Table 4). Stoichiometries of both $Ag/O_2 = 2$[8] and $Ag/O_2 = 0.5$[20] were assumed.

EDXS. The X-ray energy dispersion spectrometry (EDXS) unit on the JEOL 3000F FEG-(S)TEM was used to determine the local silver content in the catalyst particles deposited on the grid. For each catalyst a number of EDXS spectra were collected from different areas of each sample, but from the same area that the TEM images were taken. The recorded EDXS spectra were all gathered in bright field TEM mode. Furthermore, EDXS and a power spectrum obtained from Fast Fourier Transformation (FFT) of TEM images were used to give an indication on whether silver is present as metallic (Ag^0) silver or as an oxide (Ag^{2+}, Ag^+) in the imaged silver particles. With FFT, the distances in the diffraction patterns from the samples were measured and compared to the distances from the literature[23−25] obtained by X-ray diffraction measurements on silver and silver oxide.

3. Results and Discussion

3.1. HC-SCR Activity Tests. The NO to N_2 conversions and the turnover frequencies over the prepared catalysts in HC-SCR with *n*-octane are presented in Table 1. Even if the maximum conversion rates over Ag/Al_2O_3-1.28 and Ag/Al_2O_3-1.91 are almost the same in terms of reacted NO molecules per one Ag atom, the Ag/alumina catalyst with the lowest silver loading (1.28 wt %) exhibited clearly the highest activity. Vice versa the catalyst having the highest silver loading resulted in the lowest and almost nonexisting reduction activity. Moreover it can be said that the conversion over the 6.00 wt % catalyst remains below 10% at all temperatures whereas the other catalysts perform in the range of around 60−100%. Such a huge difference in activity indicates that there is a significant difference between the 6 wt % catalyst compared with the three other catalysts.

3.2. TEM. Statistical calculations on the particles measured in TEM images were used to determine the mean particle size of the silver particles on the prepared Ag/alumina catalysts (Table 2). Mean particle sizes between ca. 5 and 11 nm were recorded with high accuracy, when over 100 particles of each sample were measured. The lowest mean particle size was calculated for samples 1 (1.28 wt % Ag, MPS 5.36 nm) and 2 (1.91 wt % Ag, MPS 5.46 nm), which resulted in the highest NO_x to N_2 conversion (Table 1). The mean particle size for samples 3 (8.54 nm) and 4 (10.46 nm) is seemingly higher than the MPS calculated for catalysts 1 and 2. According to Table 1 the activity decreases with increasing silver loading and particle size, indicating that the HC-SCR activity over silver/alumina catalysts is related both to the silver loading and to the mean particle size, as also found in refs 7−9.

Figure 2a−d shows the particle size distributions for the prepared samples based on the TEM images. As can be seen from the histograms, the most frequently measured particle sizes lie noticeably lower for each sample than the mean particle size. For sample 1 the highest frequency with over 50% share corresponds to particles having a diameter of 3 nm (Figure 2a). This means that more than half of the particles in catalyst 1 are seemingly smaller than the mean particle size calculated from all of the measured particles. However, the particles fit well in the limit of lower confidence interval, which explains the big share of particles at 3 nm. On the other hand, all the prepared samples include also very large particles, up to 100 nm. Such a wide distribution of silver particles measured from TEM images has also been reported in refs 9, 11, and 12. Thus, despite the relatively low amount of big particles, the statistically calculated value of MPS is increased.

Bogdanchikova et al.[11] reported that in all the samples a low contrast shell was observed around a core of Ag metal particles, which could be attributed to a layer of oxidized silver, e.g., small oxidized silver particles. A similar feature was observed also for our samples. From Figure 4 it can clearly be seen how a low contrast area surrounds the core of a silver particle, both in bright field and dark field images. According to ref 11 the core of the particle is metallic silver. Formation of such large metallic particles, found on the samples, is likely to take place during the synthesis. Sample 2 is especially peculiar as the histogram shows (Figure 2b) that particles of 1 nm represent over 80% of all the particles measured. In addition no such big silver particles, e.g., up to 70 nm, could be detected in this sample as was the case for sample 1, which could be expected since the statistical MPS of 5.46 nm is much higher. However, the proportion of larger particles compared with the amount of smaller particles can explain the rise in the statistically calculated particle size. For sample 3 the size distribution is much wider (Figure 2c) in comparison to the size distribution for samples 1 and 2, containing a considerable amount of particles with intermediate size, e.g., around 15−40 nm. A similar widely divided size distribution pattern was also recorded for the fourth

TABLE 4: Mean Particle Sizes and Distributions Determined by O_2-Chemisorption

sample	silver content (wt %)	MPS $Ag/O_2 = 0.5$ (nm)	dispersion $Ag/O_2 = 0.5$ (%)	MPS $Ag/O_2 = 2$ (nm)	dispersion $Ag/O_2 = 2$ (%)	H_2/Ag
1	1.28	10.53	14.4	2.63	57.6	0.25
2	1.91	10.46	12.8	2.62	51.2	0.21
3	2.88	12.00	11.2	3.00	44.8	0.17
4	6.00	10.52	12.8	2.63	51.2	0.20

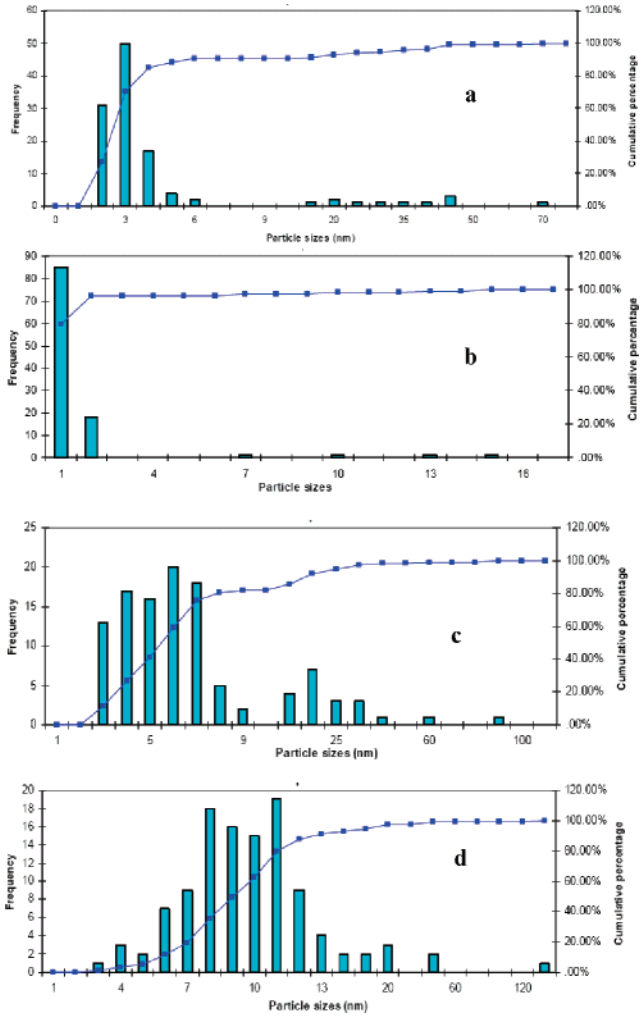

Figure 2. (a−d) Histograms presenting particle size distribution for samples 1−4 based on TEM images.

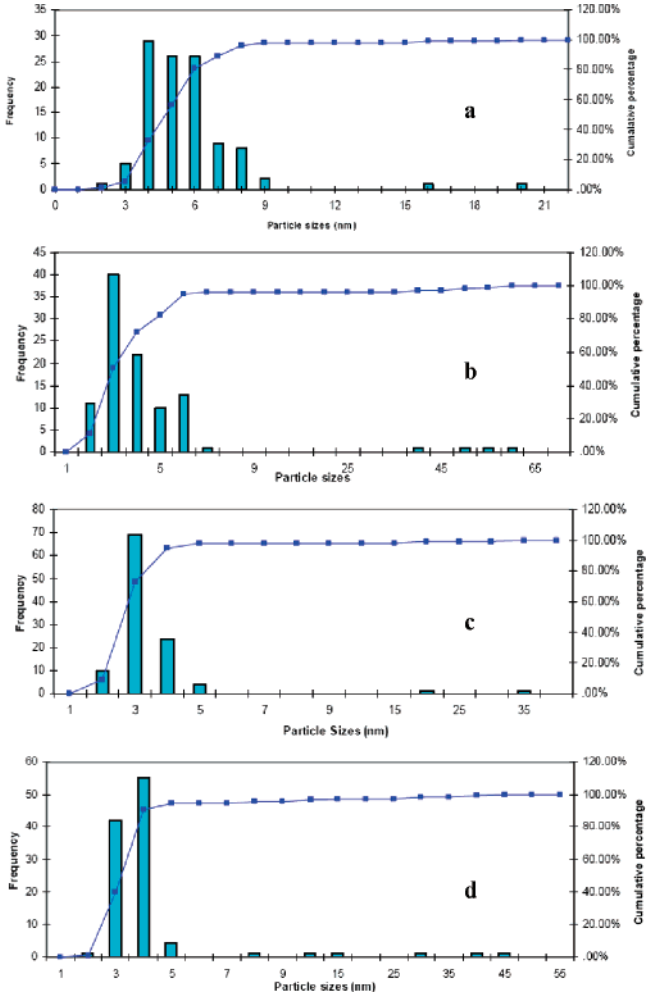

Figure 3. (a−d) Histograms presenting particle size distribution for samples 1−4 based on HAADF images.

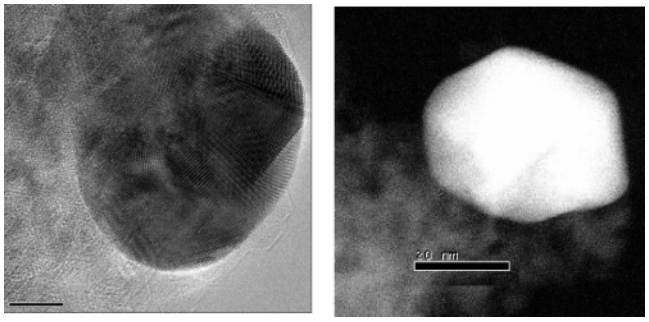

Figure 4. Low contrast area (sample 2) presenting silver oxide around the metallic silver particle found on TEM and HAADF images.

sample (Figure 2d). Note that sample 4 was the only catalyst having a significant amount of particles bigger than 100 nm. It can be concluded that the calculated MPS's for samples 3 and 4 are in analogy with the respective particle size distribution diagrams. However, based on the TEM images it should be emphasized that the particles are very heterogeneous in terms of particle size (nm) and thus general conclusions of the average particles size should be taken with care.

3.3. HAADF. When statistical calculations on the particles measured in HAADF images (Table 3) were used to determine the mean size of the silver particles, generally smaller values than from TEM images were observed (Table 2). With HAADF a considerably higher contrast between the silver and alumina was achieved (Figure 1). Due to this increase in contrast, smaller silver particles on the support could be detected. The mean particle size values for samples 1 and 2 do not differ greatly from the values recorded by TEM, but did, however, result in smaller values. The value recorded for sample 1 was also slightly smaller than the value recorded for sample 2, which is in line with the TEM results. The most significant difference in results obtained from TEM and HAADF occurs for samples 3 and 4. The mean particle size recorded for sample 3 by HAADF (3.17 nm) not only differs greatly from the value recorded by TEM (8.54 nm) but also is not in analogy with the results overall. This sample has a higher silver content than samples 1 and 2 although the mean particles size recorded by HAADF is lower. The most plausible explanation for this is that even if over 100 particles were masked, the proportion of small particles among the total amount of masked particles was much higher than the amount of bigger particles (Figure 3c).

The MPS value recorded for sample 4 is also much less than the corresponding value recorded by TEM, and surprisingly also smaller than the values recorded for samples 1 and 2. Overall it can be concluded that the mean particle sizes recorded by HAADF are very close to each other and systematically smaller than the values recorded by TEM. These results are due to the much higher contrast between silver and alumina achieved in HAADF images than in TEM images. The histograms in Figure 3a−d also support the earlier conclusion that the samples are very heterogeneous in terms of particle size, including particles from 1 to 60 nm in diameter. When comparing the particle size

distribution histograms in Figure 2a−d with those in Figure 3a−d, it can be concluded that the proportion of small particles is much higher in images taken by HAADF than by TEM. Furthermore, the MPS values received from HAADF images correspond better to peak maximums in Figure 3a−d than the MPS values recorded by TEM correspond to peak maximums in Figures 2a−d.

3.4. O_2-Chemisorption. As the MPS values determined by TEM are seemingly affected by the silver loading, in such case the dispersion of Ag on the support should also vary with varying silver loading and should be noticeable with O_2-chemisorption. However, the dispersion calculations by chemisorption are far from trivial, as stoichiometries of 0.5, 2.0, and 4.0 have been suggested in the literature.[8,20−21] In ref 21 it is proposed that surface oxide $(Ag_2O)_s$ is formed at low coverage of Ag. The oxide structure is represented by bridged Ag−O−Ag-like species, where the oxidation state of silver is monovalent (Ag^+). At higher coverage, other oxides are assumed to be formed and there might be two species, which correspond to a Ag/O ratio of one. The first one involves atomic oxygen anions, i.e., $(Ag_2O_2)_s$, the second one contains molecular oxygen of the peroxide type (AgO_2). The silver dispersions and mean particle sizes calculated according to stoichiometries of $Ag/O_2 = 2$ and $Ag/O_2 = 0.5$ are given in Table 4.

Comparing Tables 2, 3, and 4 with each other, it can be concluded that the mean particle sizes measured by applying different methods are far from being in analogy. The particle sizes determined from TEM and HAADF images are consistently larger than the particle sizes calculated with O_2-chemisorption applying stoichiometry $Ag/O_2 = 2$ and consistently smaller than the particles determined with stoichiometry $Ag/O_2 = 0.5$. However, the difference in mean particle size is smaller when comparing values obtained from TEM and HAADF with values calculated by using the stoichiometry $Ag/O_2 = 2$. Furthermore, a smaller discrepancy between results for measured MPS values is obtained when only HAADF values and chemisorption values determined for $Ag/O_2 = 2$ are compared. Particularly for sample 3, having a intermediate silver loading of 2.88 wt %, the values are very close to each other. This indicates that the stoichiometric factor 2 used in chemisorption calculation is more suitable to use for Ag/alumina catalysts than a factor of 0.5. The difference in MPS values measured from TEM and HAADF images can partly be explained by the fact that the contrast of silver and alumina in TEM images is rather similar. Thus, TEM imaging should not be used for determining the mean particle sizes of silver on alumina support, which is highly amorphous.

It should also be noted that even if more than hundred particles were masked in both cases (TEM and HAADF), all of the prepared samples are very heterogeneous in terms of silver particle sizes. Thus, if among the particles imaged there happen to be a lot of small, or alternatively big particles, then the statistically calculated, apparent MPS obviously differ from the values obtained from chemisorption. However, the confidence intervals calculated for particle sizes determined from HAADF images are narrower than confidence intervals based on TEM data. The same can be seen from the size distribution histograms, indicating that due to the increased contrast between silver and alumina, the results from HAADF imaging for this type of catalyst are much more reliable than results from TEM imaging.

Martínez-Arias et al.[9] have reported evidence of a significant increase in the size of Ag particles after the HC-SCR reaction over 1.5 and 3 wt % Ag/alumina catalysts. However, as we have shown the fresh samples are very heterogeneous in terms of particle size, including both very small and large particles. Furthermore the resolution between silver and alumina in TEM images is not the best possible. Thus, conclusions as in ref 9 based on TEM images should be taken with care.

TABLE 5: Stoichiometric Factors Calculated Based on the MPS Values Received from HAADF

sample	dispersion (%)[a]	Ag/O_2[b]
1	37	2.13
2	37	1.90
3	54	2.41
4	43	2.18

[a] The dispersion values were calculated as the number of surface atoms divided by the total number of atoms, assuming spherical particles and metallic silver, atom distance 1.43 Å according to refs 23−25. [b] Ag/O_2 calculated as the total amount of silver (mole) divided by the total amount of oxygen (mole) multiplied by the dispersion.

Still it should be emphasized that silver is mobile on the alumina support and can form larger particles or be redispersed to smaller particles, depending on whether the local reaction conditions are reducing or oxidizing and if the temperature is increasing or decreasing at the same time. This can be seen for example in the change of color (yellow or gray) of the catalyst after reduction, indicating reduction of silver species. Qu et al.[29] have also reported a significant growth of Ag particles on SiO_2 support after pretreatment at 700 °C under both O_2 and He atmosphere. In fact, the diffusion of silver atoms becomes significant at temperatures above around 480 °C (Tammann temperature). This is in analogy with the catalyst activity, which starts to decrease above 500 °C. However, the Ag/alumina catalyst is able to regain the original activity when cooled in oxygen, indicating redispersion of the sintered particles. It should also be kept in mind that the calcination temperature (550 °C, in air) then has an effect on the silver dispersion determined by chemisorption. On the other hand, the sintering of silver is inhibited by the strong interactions with the support forming highly stabilized silver oxide species.

Iglesias-Juez et al.[12] have shown that only less than 10% of silver on a calcined Ag/alumina catalyst undergo sintering during the reaction. This can be explained by the strong interactions with silver and oxygen in the support. In fact, oxygen diffusivity in silver increases exponentially with temperature and becomes significant above 500 °C.[26] Thus oxygen can be incorporated into the bulk lattice of silver when the catalyst is treated with oxygen at high temperatures. Thus it is reasonable to believe that calcination of the catalysts at 550 °C in air leads to formation of strongly bound, possible subsurface oxygen species. Such strongly bound Ag-O species are hard to reduce at mild conditions prior to the O_2-chemisorption. Therefore, the results are valid only for the specific pretreatment conditions and should not be compared with results where either a noticeably different temperature for calcination or another pretreatment condition has been used.

As revealed earlier, the stoichiometric factor for oxygen chemisorption on silver is not unarguable and obviously depends on the conditions (temperature) at which the sample has been reduced prior to the oxygen adsorption. Thus we have calculated the experimental stoichiometric factors based on the MPS received from HAADF imaging (assuming spherical particles). In Table 5 the amount of silver atoms needed for one oxygen molecule to adsorb is given. As can be seen, the experimental stoichiometric factor for each sample is very close to 2, meaning that one oxygen molecule adsorbes roughly on two silver atoms. Moreover, the values are very close to the stoichiometric value $Ag/O_2 = 2$ as suggested in refs 8 and 20. These results support

TABLE 6: Quantification Results from EDXS Spectra

sample	EDXS no.	atomic Ag (%)	atomic Al (%)	atomic O (%)	Ag (wt %)	Al (wt %)	O (wt %)
1	1	2.36	35.93	61.71	11.53 ± 2.10	43.83 ± 1.84	44.64 ± 2.01
	2	0.04	34.25	65.71	0.22 ± 1.19	46.67 ± 1.47	53.10 ± 1.50
	3	7.90	36.60	55.50	31.24 ± 1.73	36.20 ± 1.25	32.56 ± 1.42
	4	0.39	41.47	58.14	2.00 ± 0.78	53.51 ± 1.20	44.49 ± 1.19
	5	0.13	37.17	62.73	0.70 ± 1.26	49.61 ± 1.59	49.69 ± 1.60
2	1	0.30	36.23	63.47	1.61 ± 0.95	48.26 ± 1.61	50.13 ± 1.64
	2	0.46	34.92	64.61	2.47 ± 1.94	46.51 ± 2.80	51.02 ± 2.89
	3	0.59	36.95	62.46	3.09 ± 1.36	48.39 ± 2.10	48.51 ± 2.15
	4	0.23	39.36	60.41	1.22 ± 1.14	51.72 ± 1.39	47.06 ± 1.38
	5	42.10	27.90	30.00	78.65 ± 0.49	13.04 ± 0.31	8.31 ± 0.40
3	1	1.38	35.81	62.81	7.01 ± 1.52	45.58 ± 1.58	47.41 ± 1.68
	2	0.47	34.72	64.81	2.50 ± 2.41	46.28 ± 2.80	51.22 ± 2.91
	3	0.94	36.34	62.72	4.86 ± 1.07	47.01 ± 1.26	48.12 ± 1.31
	4	0.38	37.09	62.53	2.03 ± 0.32	48.99 ± 0.43	48.98 ± 0.43
	5	0.62	34.97	64.42	3.27 ± 1.32	46.23 ± 1.27	50.50 ± 1.32
4	1	0.23	35.95	63.82	1.24 ± 2.38	48.12 ± 2.60	50.64 ± 2.66
	2	1.34	41.73	56.93	6.62 ± 2.44	51.62 ± 3.04	41.75 ± 3.12
	3	0.50	36.93	62.57	2.64 ± 1.52	48.57 ± 1.58	48.79 ± 1.62
	4	1.17	36.51	62.32	6.00 ± 1.60	46.72 ± 1.43	47.28 ± 1.48
	5	0.73	37.31	61.95	3.81 ± 1.10	48.47 ± 1.34	47.72 ± 1.38

our earlier conclusion, based on the comparison of mean particle values from TEM, HAADF, and O_2-chemisorption applying $Ag/O_2 = 2$, that 2 is a more suitable stoichiometric factor to be used than 0.5 or 4 as also suggested in the literature[8,20−21] if the pretreatment of the catalyst and the oxygen adsorption have been performed under similar conditions as in this study.

3.5. EDXS. As the TEM/HAADF images demonstrated a very heterogeneous silver distribution on the support, EDXS was applied to study the local silver dispersion in addition to the global dispersion determined by O_2-chemisorption. Table 6 gives the silver dispersion as percent atomic silver and as weight percent silver. EDXS is a very accurate quantitative method but the uncertainty in the quantification increases if the local silver content is low. This is obvious from the standard deviations, which for the silver content are quite high. However, it can be concluded that the silver content varies largely depending on from which part of the sample the spectrum is collected. This supports the conclusion from TEM and HAADF images that regardless of the silver loading on the support, the silver dispersion is highly nonuniform, indicating the silver dispersion depends on the support properties rather than on the preparation method.

As stated in the Introduction the catalytic activity is highly dependent on the Ag loading with the best activity found at intermediate concentrations, e.g., 2−3 wt %[7−12,18] depending on the preparation method and the type of alumina used as a support. Bethke et al.[7] attributed the difference in catalytic behavior to a much higher dispersion of silver on the 2 wt % catalyst than on the 6 wt % catalyst and that the oxidation states of Ag were different under reaction conditions. On the basis of Figure 3a−d, presenting data for the fresh calcined samples having a silver loading between 1.28 and 6.00 wt %, it can be concluded that the particle size distributions do not vary in such a significant way that they could explain the great difference in activities. It indicates that the activity is related rather to the state of silver than to the particle size. The results presented in Tables 3−5 also clearly show that no linear dependence between silver loading and dispersion can be manifested.

A specific EDXS scan made for a large silver particle (sample 1) detected in a TEM image (Figure 5) shows a silver content of 99.41 wt % (±1.25), 0.26 wt % (±0.58) alumina, and 0.33 wt % (±1.12) oxygen. The unlabeled peaks in Figure 5 are from the carbon film and the copper grid. This indicates that metallic silver is predominant in large particles. Additionally a power spectrum was acquired by FFT operations from Figure 6b, which is from the area surrounded by a gray square in Figure 6a. It was then used to identify silver and its oxides. The reciprocal distances (given as the distance from the center of the diffraction pattern out to the diffraction spots) measured in Figure 6 equal the following *d*-values: 1.43, 1.81, 2.02, 2.31, and 2.44 Å. If the distances are compared to the distances given in refs 23−25 it can be seen that the first distance (1.43 Å) corresponds quite well to the (220) reflection for Ag and the (311) reflection for cubic Ag_2O. It is also close to the (103) reflection for hexagonal Ag_2O (1.40 Å). The second measured distance (1.81 Å) is in agreement with the (102) reflection for hexagonal Ag_2O. The third distance (2.02 Å) is very close to the (200) reflection for Ag (2.04 Å). The 2.31 Å value is almost identical with the (101) reflection for hexagonal Ag_2O (2.33 Å), but it is also close to the (111) reflection for Ag (2.36 Å) and the (200) reflection

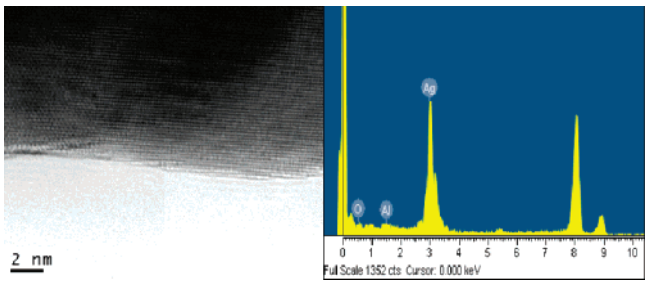

Figure 5. TEM image on a large particle and the corresponding EDXS spectrum.

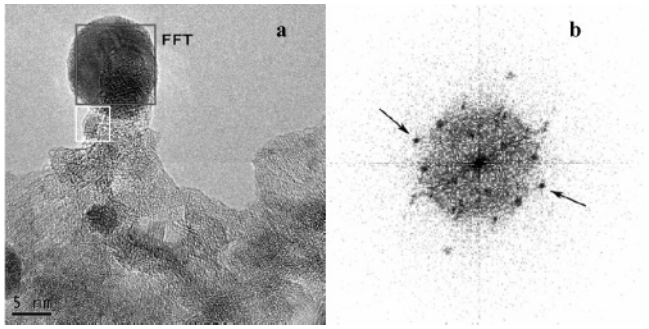

Figure 6. (a,b) Power spectra acquired from Digital Micrograph and the corresponding HRTEM image from sample 1. The area upon which the FFT was performed is marked with a gray square. The distance between the arrows in the power spectra equals 9.9 nm^{-1}.

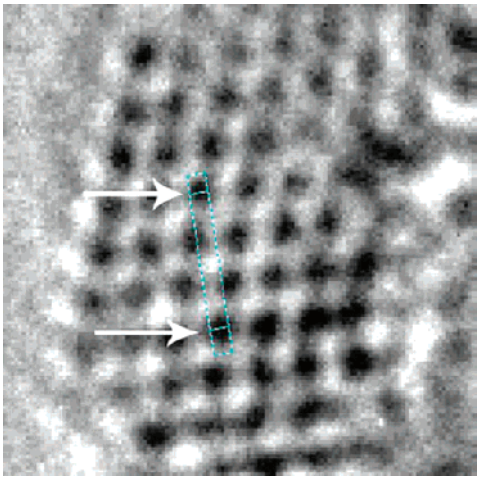

Figure 7. The size of the particle in the image is approximately 2 nm viewed along the [110] direction. The arrows mark out the space diagonal in the unit cell equal to 7.26 $Å^{-1}$.

for cubic Ag_2O (2.37 Å). The last measured distance (2.44 Å) is closest to the *d*-values for AgO (111), Ag (111), and cubic Ag_2O (200). On the basis of the results from FFT it can be concluded that both metallic silver and silver oxide phases are present in sample 1. Moreover it can be said that the fact that (101), (102), and (103) reflections for hexagonal silver oxide were identified indicates that hexagonal Ag_2O is present in sample 1. The (111), (200), and (220) reflections for Ag explain the *d*-values, indicating that also metallic Ag is present, meanwhile AgO and cubic Ag_2O are unlikely. Furthermore, the particle in Figure 6a is around 10 nm, e.g., much smaller than the particle in Figure 5, which also supports the previous statement that silver oxide is more likely the predominant phase in small silver particles, whereas large particles consist of metallic silver. However, the conclusion that large particles in calcined non-reduced catalysts consist of metallic silver and small particles of silver oxide is not unequivocal. In Figure 7 the area surrounded by a white square in Figure 6a is enlarged. It shows atomic distances and angles consistent with a cubic unit cell with $a_0 = 4.2$ Å. This corresponds to the cubic unit cell for metallic silver, which has a cell edge a_0 equal to 4.1 Å. This gives evidence that small (~2 nm) metallic silver particles also can exist on the alumina support.

3.6. Activity vs Metal Loading. As has been shown above, different characterization methods (O_2-chemisorption, HRTEM, and HAADF) result in different values in metal dispersion and mean particle size for Ag/alumina samples with varying silver loading. Thus a combination of these methods should be used to obtain a realistic picture of the size of the silver particles and their distribution on alumina. However, the relatively small differences in MPS values obtained by characterizing the samples with the methods applied in this study cannot explain the great variation in NO_x to N_2 reduction activities over the catalysts. Hence, there is a reason to believe that it is rather the state of silver (Ag^0, Ag^+, or Ag^{2+}) that is the determining factor when relating the activity to metal loading.

Small metallic silver clusters ($Ag_n^{\delta+}$), formed by addition of hydrogen, have been reported to be responsible for the NO to N_2 activity increase in the presence of hydrogen.[30−35] Satokawa et al.[31] were the first to report bands at 260 and 284 nm, ascribed to small $Ag_n^{\delta+}$ clusters, in the UV−vis spectrum of Ag-ZSM-5. Small $Ag_n^{\delta+}$ with $n = 2-4$ were also revealed in Ag-ZSM-5 by ex situ EXAFS measurements[31] carried out after the H_2/C_3H_8-SCR-NO_x reaction. In ref 35 it is shown that small silver clusters, $n \leq 8$, can be found in both the absence and the presence of hydrogen. As a matter of fact, the cluster formation is connected to the NO to N_2 conversion activity as described in ref 35. Thus it cannot be concluded that clusters would be directly formed due to direct interactions with hydrogen. In ref 36 Brosius et al. suggested that at low temperatures hydrogen reduces the nitrates bound to the silver thus reducing the Ag(I) to Ag(0). It is possible that after the reduction metallic silver can form small clusters. Another observation that supports this conclusion is that when the reduction activity over the catalyst is high, clusters are detected even in the absence of hydrogen.[35] High activity over the catalyst requires temperatures ≥400 °C, i.e., temperatures where the thermal decomposition of silver nitrate occurs.[11] At temperatures over 400 °C oxidation of hydrocarbon is considerably high, implying that reduction of the surfaces is possible.

However, as shown in this study, both metallic silver and silver oxides can be found on the fresh oxidized samples. Thus it can be concluded that based on the characterization done ex situ, i.e., not in the real reaction conditions, activity and metal loading cannot be directly related. In ref 18 it is shown that on the samples with high metal loading (>2.88 wt %) silver does not redisperse after reduction to silver oxide to the same extent as on the samples with metal loadings equal to or less than 2 wt %, which happens in real conditions where silver is locally reduced by hydrocarbon or hydrogen (if used) to metallic silver. This can be a factor in explaining why no clear difference between the samples can be found in ex situ characterization, but in real reaction conditions the behavior of the catalysts in terms of NO_x to N_2 reduction activity is totally different. Hence, it can be concluded that for the explanation of the dependence between activity and metal loading, all characterization should be performed in situ under real reaction conditions.

4. Conclusions

The difference in mean particle sizes, particle size distribution, and dispersion for four fresh (calcined) Ag/Al_2O_3 catalysts with different metal loadings was determined by means of HRTEM, HAADF, O_2-chemisorption, and EDXS. The different silver loading on the prepared catalysts did not result in significant variations in dispersion determined by O_2-chemisorption. The mean particle size values (MPS) determined by HRTEM resulted in increasing MPS value with increasing metal loading as expected. However, when the particle sizes were determined by HAADF imaging, providing considerably better contrast between silver and alumina, a linear dependence between particle size and metal loading could not be statistically manifested. For all samples it was found that silver is very heterogeneously distributed on the support, e.g., both small and very large particles were found on each sample. However, the great difference between the activities over the prepared samples could not be explained with variations in mean particle size or particle size distribution. Additionally, EDXS results revealed that the large particles on the prepared samples consisted mainly of metallic silver. Moreover it was found that hexagonal silver oxide (Ag_2O) is the most likely compound to be present on the samples. Finally it can be concluded that in situ characterization is needed for obtaining a clean-cut structure−reactivity relationship for this type of catalyst.

Acknowledgment. The financial support from the European Union through the Ammonore project (GR5D-CT 2001-00595) and from the Graduate School of Materials Research is gratefully acknowledged. This work is part of the activities at the Åbo Akademi Process Chemistry Centre within the Finnish Centre

of Excellence Programme (2000−2005) by the Academy of Finland. The authors from Lund University acknowledge the Swedish Research Council for support.

References and Notes

(1) Iwamoto, M.; Yahiro, H.; Shundo, S.; Yu-u, Y.; Mizuno, N. *Appl. Catal.* **1991**, *70*, 15.

(2) Held, W.; Koenig, A.; Richter, T.; Puppe, L. *SAE Paper* **1990**, 900496.

(3) Miyadera, K. *Appl. Catal. B* **1993**, *2*, 199.

(4) Burch, R.; Millington, P. J. *Catal. Today* **1996**, *29*, 37.

(5) Fritz, A.; Pitchon, V. *Appl. Catal. B* **1997**, *13*, 1.

(6) Burch, R.; Breen, J. P.; Meunier, F. C. *Appl. Catal. B* **2002**, *39*, 283.

(7) Bethke, K. A.; Kung, H. H. *J. Catal.* **1997**, *172*, 93.

(8) Hoost, T. E.; Kudla, R. J.; Kollins, K. M.; Chattha, M. S. *Appl. Catal. B* **1997**, *13*, 59.

(9) Martínez-Arias, A.; Fernández-García, M.; Iglesias-Juez, A.; Andersson, J. A.; Conesca, J. C.; Soria, J. *Appl. Catal. B* **2000**, *28*, 29.

(10) Shimizu, K.-i.; Shibata, J.; Yoshida, H.; Satsuma, A.; Hattori, T. *Appl. Catal. B* **2001**, *30*, 151.

(11) Bodganchikova, N.; Meunier, F. C.; Avalos-Borja, M.; Breen, J. P.; Pestryakov, A. *Appl. Catal. B* **2002**, *36*, 287.

(12) Iglesias-Juez, A.; Hungría, A. B.; Martínez-Arias, A.; Fuerte, A.; Fernández-García, M.; Anderson, J. A.; Conesa, J. C.; Soria, J. *J. Catal.* **2003**, *217*, 310.

(13) Eränen, K.; Lindfors, L.-E.; Niemi, A.; Elfving, P.; Cider, L. *SAE Paper* **2000**, 2000-01-2813.

(14) Luo, Y.; Hao, J.; Hou, Z.; Fu, L.; Li, R.; Ning, P.; Zheng, X. *Catal. Today* **2004**, *93*−*95*, 797.

(15) Eränen, K.; Lindfors, L.-E.; Klingstedt, F.; Murzin, D. Yu. *J. Catal.* **2003**, *219*, 25.

(16) Klingstedt, F.; Eränen, K.; Lindfors, L.-E.; Andersson, S.; Cider, L.; Landberg, C.; Jobson, E.; Eriksson, L.; Ilkenhans, T.; Webster, D. *Top. Catal.* **2004**, *30*/*31*, 27.

(17) Eränen, K.; Klingstedt, F.; Arve, K.; Lindfors, L.-E.; Murzin, D. Yu. *J. Catal.* **2004**, *227*, 328.

(18) Arve, K.; Capek, L.; Klingstedt, F.; Eränen, K.; Lindfors, L.-E.; Murzin, D. Yu.; Dedecek, J.; Sobalik, Z.; Wichterlová, B. *Top. Catal.* **2004**, *30*−*31*, 91.

(19) Furusawa, T.; Seshan, K.; Lercher, J. A.; Lefferts, L.; Aika, K.-i. *Appl. Catal. B* **2002**, *37*, 205.

(20) Carlo Erba Instruments, Instruction Manual, 1990.

(21) Golodets, G. I. *Heterogeneous Catalytic Reactions Involving Molecular Oxygen*; Studies in Surface Science and Catalysis, No. 15; Elsevier: Amsterdam, The Netherlands, 1983.

(22) Liu, J. *Microsc. Microanal.* **2004**, *1*, 55.

(23) Powder Diffraction File—Inorganic Phases, alphabetical index, 1985; JCPDS International Centre for Diffraction Data, 1985; Newton Square, PA.

(24) Powder Diffraction File, sets 1−5, 4-0783, 4-0875, 4-0880, 1974; JCPDS International Centre for Diffraction Data, 1985; Newton Square, PA.

(25) Powder Diffraction File, Microfich sets 1−30, 12-793, 19-1155 (Kabalkina et al. *Sov. Phys. Dokl.* **1964**, *8*, 972−974), 22-472; JCPDS International Centre for Diffraction Data, 1985; Microfich Housing Frame Iowa.

(26) Datey, A. K.; Smith, D. J. *Catal. Rev. Sci. Eng.* **1992**, *34*, 129.

(27) Jose-Yacaman, M.; Avalos-Borja, M. *Catal. Rev. Sci. Eng.* **1992**, *34*, 55.

(28) Thomas, J. M.; Terasaki, O.; Gai, P. L.; Zhou, W. Z.; Gonzales-Calbet, J. *Acc. Chem. Res.* **2001**, *34*, 583.

(29) Qu, Z.; Cheng, M.; Huang, W.; Bao, X. *J. Catal.* **2005**, *229*, 446.

(30) Satokawa, S. *Chem. Lett.* **2000**, 294.

(31) Satokawa, S.; Shibata, J.; Shimizu, K.; Satsuma, A.; Hattori, T. *Appl. Catal. B* **2003**, *42*, 179.

(32) Shibata, J.; Shimizu, K.; Satokawa, S.; Satsuma, A.; Hattori, T. *Phys. Chem. Chem. Phys.* **2003**, *5*, 2154.

(33) Shibata, J.; Takada, Y.; Shichi, A.; Satokawa, S.; Satsuma, A.; Hattori, T. *J. Catal.* **2004**, *222*, 368.

(34) Shabata, J.; Shimizu, K.; Takada, Y.; Shichi, A.; Yoshida, H.; Satokawa, S.; Satsuma, A.; Hattori, T. *J. Catal.* **2004**, *227*, 367.

(35) Sazama, P.; Čapek, L.; Drobná, H.; Sobalík, Z.; Dědeček, J.; Arve, K.; Wichterlová, B. *J. Catal.* **2005**, *232*, 302.

(36) Brosius, R.; Arve, K.; Groothaert, M. H.; Martens, J. A. *J. Catal.* **2005**, *231*, 344.